SERCA Structural Dynamics Induced by ATP and Calcium†

Benjamin Mueller, Min Zhao, Igor V. Negrashov, Roberta Bennett, and David D. Thomas*

Department of Biochemistry, Molecular Biology, and Biophysics, University of Minnesota Medical School, Jackson Hall 6-155, 312 Church Street, Minneapolis, Minnesota 55455

Received May 24, 2004; Revised Manuscript Received July 13, 2004

ABSTRACT: We have used time-resolved phosphorescence anisotropy (TPA) to probe rotational dynamics of the rabbit skeletal sarcoplasmic reticulum Ca-ATPase (SERCA), to test the hypothesis, generated from X-ray crystallography, that large-scale structural changes are induced by Ca in this system. Previous TPA studies on SERCA used primarily erythrosin 5′-isothiocyanate (ErITC), which binds to the nucleotide-binding domain and inactivates the enzyme. To investigate rotational dynamics of the active enzyme, we labeled SERCA with erythrosin 5′-iodoacetamide, which binds to the phosphorylation domain and has a minimal effect on the calcium-dependent ATPase activity. In the absence of nucleotide and the presence of calcium, TPA results were similar to those observed previously with ErITC, consistent with the global uniaxial rotation of SERCA monomers and oligomers and small amplitude internal protein dynamics. The removal of Ca had only a slight effect, while the addition of adenosine 5′-triphosphate (ATP) increased the amplitude of internal dynamics and changed the probe's orientation, corresponding to tilting of the phosphorylation domain by at least 20°. Ca partially reversed the ATP effects. A nonhydrolyzable ATP analogue had the same effects as ATP, showing that the observed changes were not dependent on active ion transport. Computational analysis indicates that these ligands affect primarily the internal dynamics of the enzyme, with negligible effects on global dynamics and enzyme association. Melittin, which has been shown to aggregate and inhibit SERCA, eliminated the nucleotide-induced internal dynamics and increased the final anisotropy. We propose that (i) the large Ca-dependent structural changes suggested by SERCA crystallography are more dependent on ATP than on Ca and (ii) aggregation-induced inhibition of SERCA is due to the functional coupling between global and internal protein dynamics.

Sarco/endoplasmic reticulum Ca-ATPase (SERCA),[1] an integral membrane protein of sarcoplasmic reticulum (SR), transports calcium actively from the cytoplasm into the SR lumen and thereby relaxes muscle at the expense of adenosine 5′-triphosphate (ATP) hydrolysis (*1*). A widely accepted kinetic scheme of the enzymatic reaction involves cycling between two global conformations, E1 (high Ca affinity) and E2 (low Ca affinity). Crystal structures proposed to correspond to both states have been determined (*2*, *3*) and have been interpreted to suggest that Ca induces large domain movements in SERCA, including substantial tilting of the phosphorylation domain. However, the relationships between these structures and those occurring during the catalytic cycle under physiological conditions remain to be elucidated. Additional internal structural changes have been proposed to occur during the catalytic cycle, for example, due to ATP binding, hydrolysis, and phosphoenzyme formation (*4*−*6*).

The detection of SERCA structural transitions under physiological conditions requires spectroscopy (*2*, *7*−*10*). Previous time-resolved phosphorescence anisotropy (TPA) studies in this laboratory have established that SERCA activity and regulation are quite dependent on microsecond molecular dynamics and protein−protein interactions (*9*, *11*, *12*). In previous TPA studies on this system using erythrosin 5′-isothiocyanate (ErITC), we have shown that SERCA self-association is strongly correlated with the inhibition of enzymatic activity (*10*, *13*−*15*) and that in cardiac SR, phosphorylation of phospholamban correlates with the release of inhibitory self-association of SERCA (*15*). However, this method of labeling SERCA strongly inhibits the activity of this enzyme, preventing direct correlation of SERCA activity and rotational dynamics (*10*).

It has been shown previously that a thiol-directed iodoacetamide spin label, specific for Cys 674 on the P domain, can be used to detect SERCA dynamics during function without inhibiting the enzyme and that it reveals conformational changes in response to ATP and Ca (*16*, *17*). Unfortunately, that spin label is sensitive only to nanosecond (internal) dynamics, not to microsecond (global) dynamics. Saturation transfer electron paramagnetic resonance (EPR)

† This work was supported by a research grant to D.D.T. from the National Institutes of Health (GM27906). B.M. was supported by predoctoral fellowships from the Lillehei Heart Institute and, subsequently, the American Heart Association.

* To whom correspondence should be addressed. Tel: 612-625-0957. Fax: 612-624-0632. E-mail: ddt@umn.edu.

[1] Abbreviations: AMPPCP, adenylyl [β,γ-methylene]diphosphonate; ATP, adenosine 5′-triphosphate; BSA, bovine serum albumin; Ca, free Ca^{2+} concentration; Ca-ATPase, Ca^{2+}/Mg^{2+}-dependent ATPase; EGTA, ethylene glycol bis(β-aminoethyl ether)-*N*,*N*,*N*′,*N*′-tetraacetic acid; ErIA, erythrosin 5′-iodoacetamide; ErITC, erythrosin 5′-isothiocyanate; IAEDANS, 5-((((2-iodoacetyl)amino)ethyl)amino)naphthalene-1-sulfonic acid; MOPS, 3-(*N*-morpholino)propanesulfonic acid; SDS−PAGE, sodium dodecyl sulfate polyacrylamide gel electrophoresis; SERCA, sarco/endoplasmic reticulum Ca-ATPase; SR, sarcoplasmic reticulum; TPA, time-resolved phosphorescence anisotropy.

10.1021/bi0489457 CCC: $27.50
Published on Web 09/18/2004

of a maleimide spin label was shown to be sensitive to microsecond dynamics, but that measurement had insufficient resolution to resolve internally from global dynamics. Therefore, in the present study, we have labeled SERCA with a sulfhydryl-directed phosphorescent probe, erythrosin 5′-iodoacetamide (ErIA). This probe was used unsuccessfully in a prior study of SERCA TPA (*18*), probably because of overlabeling. In the present study, we have used a protocol that labels the enzyme specifically on the P domain and minimally interferes with the calcium-dependent ATPase activity (*9*). We show below that, unlike probes used previously, ErIA gives TPA signals that are sensitive to both ATP and Ca binding and reports both internal and global rotational dynamics of SERCA during active calcium pumping. Perturbation of this system by the SERCA-aggregating peptide melittin reveals functional coupling between global and internal dynamics.

MATERIALS AND METHODS

Reagents and Solutions. ErIA and 5-((((2-iodoacetyl) amino) ethyl) amino) naphthalene-1-sulfonic acid (IAEDANS) were purchased from Molecular Probes, Inc. (Eugene, OR). Adenylyl [β,γ-methylene]diphosphonate (AMPPCP) and phosphoenol pyruvate were obtained from Boehringer Mannheim, Inc. (Indianapolis, IN). Bovine serum albumin (BSA), ATP, β-nicotinamide adenine dinucleotide (NADH), pyruvate kinase, lactate dehydrogenase, catalase, glucose oxidase type IX, and β,D-glucose were products of Sigma Chemical, Inc. (St. Louis, MO). Ionophore A23187 was purchased from Calbiochem, Inc. (San Diego, CA). Reagents for sodium dodecyl sulfate polyacrylamide gel electrophoresis (SDS−PAGE) (4−15% gradient Tris-Glycine Ready Gels, polyacrylamide precast minigels, and running buffer) and the molecular weight standards were obtained from Bio-Rad Laboratories (Richmond, CA).

Preparations and Assays. SR vesicles were prepared from fast-twitch skeletal muscle of New Zealand White rabbits (*19*) and purified on a discontinuous sucrose gradient (*20*) to remove junctional SR-containing calcium release channels. The resulting light SR was harvested and suspended in sucrose buffer [0.3 M sucrose, 20 mM 3-(N-morpholino)-propanesulfonic acid (MOPS), 1.0 mM NaN_3, pH 7.0] and flash-frozen and stored in liquid nitrogen until use. Protein concentrations were measured by the Biuret method (*21*) using BSA as a standard, with a SERCA molecular mass of 110 kDa. Calcium-dependent ATPase activity was assayed at 25 °C using an NADH-detecting enzyme-linked method (*22*).

Labeling and Sample Preparation. SR (1.0 mg protein per mL) was labeled with 10.2 μM ErIA at 4 °C in labeling buffer (30 mM MOPS, 1 mM $MgCl_2$, 100 mM KCl, pH 6.8). After 2.5 h of reaction, 1.4 mg/mL BSA was added to scavenge unreacted dye for 20 min on ice. The solution was then centrifuged for 20 min at 66000*g* at 4 °C, and the pellet was rinsed with ice-cold sucrose buffer before homogenization. The concentration of bound ErIA was calculated using absorbance at 532 nm and an extinction coefficient of 74000 M^{-1} cm^{-1} (*10*). Specific labeling of SERCA was verified by scanning an unstained SDS polyacrylamide gel using a fluorescence imaging device (*9*).

Time-Resolved Phosphorescence Spectroscopy. The instrumentation and experimental procedure used to record TPA and total intensity have been described in detail previously (*10*, *23*). The TPA decay $r(t)$ is defined as

$$r(t) = \frac{I_v(t) - GI_h(t)}{I_v(t) + 2GI_h(t)} \quad (1)$$

where $I_v(t)$ and $I_h(t)$ are the phosphorescence intensities observed through a polarizer oriented vertically and horizontally, respectively, following the vertically polarized excitation laser pulse. G is an instrumental correction factor determined by assuming that the final anisotropy is zero for ErIA-labeled BSA in glycerol. TPA of ErIA-labeled SERCA was routinely collected and signal-averaged for 10 loops, each consisting of 1000 acquisitions of $I_{vv}(t)$ and $I_{vh}(t)$ with a laser repetition rate of 100 Hz.

Oxygen was removed from the sample prior to data collection by incubation with 100 μg/mL glucose oxidase, 15 μg/mL catalase, and 5 μg/mL β,D-glucose for 10 min. For −Ca experiments, 0.25 ± 0.05 mg/mL of ErIA-labeled SERCA was added to a sealed cuvette (0.3 cm × 1.0 cm) containing standard TPA buffer [20 mM MOPS, 80 mM KCl, 1.0 mM $MgCl_2$, 0.1 mM ethylene glycol bis(β-aminoethyl ether)-*N*,*N*,*N*′,*N*′-tetraacetic acid (EGTA), pH 7.0]. For +Ca experiments, 0.103 mM $CaCl_2$ was added, to produce 10 μM Ca. The [Ca^{2+}] concentration was calculated using the Chelator program (*24*).

TPA Data Analysis. All data sets were fitted using nonlinear least squares minimization software written by I. V. N. In some cases, global analysis was performed by simultaneously fitting several data sets and treating one or more parameters as "linked" (assuming the same value for all data sets). The goodness of fit was evaluated from χ^2 values (Marquardt−Levenberg algorithm) and a plot of the residual (data minus fit). Phosphorescence decays [unpolarized, calculated as $I(t) = I_v(t) + 2GI_h(t)$] were analyzed by fitting $I(t)$ to a sum of n exponentials

$$I(t) = \sum_{i=1}^{n} I_i \exp^{-t/\tau_i} \quad (2)$$

where τ_i is the triplet excited state lifetime.

TPA decays were analyzed using a model-independent sum of exponentials plus a constant

$$r(t) = \sum_{i=1}^{n} r_i \exp^{-t/\phi_i} + r_\infty \quad (3)$$

where ϕ_i is a rotational correlation time and r_∞ is the final anisotropy.

The observed initial anisotropy r_o obtained by fitting eq 3 (at $t = 0$) is less than or equal to the theoretical maximum value r_{max}, as expressed by

$$r(0) = r_o = r_{max}S^2,\ r_{max} = 0.4\,P_2(\cos\delta),\quad P_2(x) = 1.5x^2 - 0.5 \quad (4)$$

where δ is the angle between the absorption and the emission transition dipoles of the probe [see ref (*25*) for illustration of probe angles]. The value of r_{max} for ErIA, determined from the anisotropy of the dye immobilized in a PMMA block, is 0.205 (*26*), corresponding to $\delta = 34.8°$. δ was fixed to this

value for fitting of all data sets. S is the order parameter that describes the rapid internal protein motions that decrease the initial anisotropy from r_{max} to r_o. The angular amplitude of this rapid motion can be calculated from

$$\theta_c = \cos^{-1}[-0.5 \pm 0.5\sqrt{1+8S}] \quad (5)$$

where θ_c is the half-cone angle for rapid submicrosecond probe wobble.

To obtain a more explicit molecular interpretation of the TPA data, we used a model of uniaxial rotational diffusion (*27*), which has been successfully applied to describe TPA decays from many membrane proteins, including ErITC-labeled SERCA (*10*), discussed in detail by Mersol et al. (*25*). The anisotropy decay is given by

$$r(t) = x_1 r_0 + \sum_{i=1}^{n} x_i r_i(t), \quad x_1 + \sum_{i=1}^{n} x_i = 1$$
$$r_i(t) = S^2(a_\alpha e^{-4D_i t} + a_\beta e^{-D_i t} + a_\gamma) \quad (6)$$

where x_1 is the mole fraction of immobile proteins, x_i is the mole fraction of uniaxially rotating species i having rotational diffusion coefficient D_i, and

$$a_\alpha = 1.2\ (\sin\theta_a \cos\theta_a \sin\theta_e \cos\theta_e \cos\psi_{ae})$$
$$a_\beta = 0.3\ (\sin^2\theta_a \sin^2\theta_e \cos 2\psi_{ae})$$
$$a_\gamma = 0.4\ P_2(\cos\theta_a)\ P_2(\cos\theta_e) \quad (7)$$

θ_a (θ_e) is the polar angle between the absorption (emission) transition dipole and the normal to the membrane plane, and ψ_{ae} is the relative azimuthal orientation of the two dipoles. ψ_{ae} was eliminated by substituting the expression (*25*)

$$\cos\psi_{ae} = \frac{\cos\delta - \cos\theta_a \cos\theta_e}{\sin\theta_a \sin\theta_e} \quad (8)$$

D is the rotational diffusion coefficient, as defined by the Saffman−Delbrück equation

$$D = \frac{kT}{4\pi a^2 h\eta} \quad (9)$$

where a is the effective cylindrical radius of the protein immersed within the membrane, h is the membrane thickness, η is the viscosity of the membrane, k is the Boltzmann constant, and T is the absolute temperature (K). In skeletal SR at 4 °C, it has been shown that $a^2D = 9.3$ Å$^2/\mu$s (*10*), so a SERCA monomer ($a = 28$ Å) should have $D \approx 10^4$ s^{-1}, giving rise to correlation times of $1/(4D) = 25$ μs and $1/D = 100$ μs. Any decrease in D, without a change in lipid fluidity, is evidence for protein aggregation.

RESULTS

Characterization of ErIA-Labeled SERCA. The labeling stoichiometry was measured to be 0.9 ± 0.1 dye bound per SERCA. The ErIA-labeled enzyme prepared in this manner retained 75 ± 5% of the calcium-dependent ATPase activity of unlabeled SR. Quantitative analysis of the densitometric scan of SR proteins separated by SDS−PAGE prior to Coomassie staining indicated that 98 ± 2% of the erythrosin dye migrated with SERCA, consistent with previous results that showed highly specific labeling of SERCA in SR membranes with ErIA (*9*). To further determine the specificity of ErIA labeling, we measured labeling competition between ErIA and IAEDANS, which reacts primarily with Cys-674 of SERCA (*20*, *28*); for IAEDANS labeling protocol, see ref (*29*). One equivalent of reacted IAEDANS reduced subsequent ErIA labeling by 80−90%, and one equivalent of reacted ErIA reduced subsequent IAEDANS labeling by 70−80%. Thus, ErIA reacts primarily with Cys-674 in the P domain.

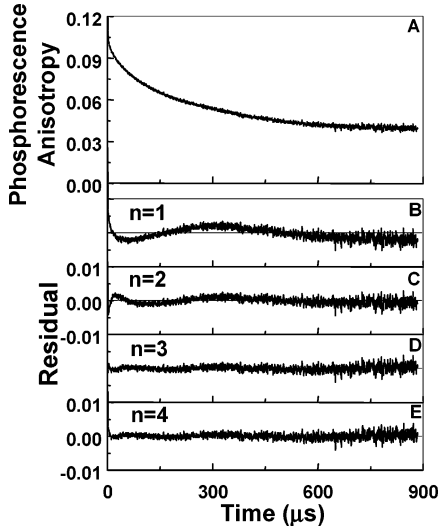

FIGURE 1: Phosphorescence anisotropy of ErIA-labeled SERCA ("-Ca", panel A) is best fitted by a three-exponential decay (eq 3, $n = 3$). Plots of residuals (panels B−E) indicate the goodness of fit for one ($\chi^2 = 8.76$), two ($\chi^2 = 2.61$), three $\chi^2 = 0.68$), and four ($\chi^2 = 0.68$) exponentials, respectively.

Phosphorescence Intensity Decay. Analysis of the total (unpolarized) phosphorescence emission intensity ($I_{vv} + 2GI_{vh}$) of ErIA-labeled SERCA indicated that three lifetimes were necessary and sufficient to fit the decay adequately (eq 2, $n = 3$). The values of the ErIA lifetimes were similar to those previously reported for ErITC bound to SERCA (*10*). ATP and Ca had negligible effects on these lifetimes.

Model-Independent Analysis of TPA in the Absence of ATP and Ca. Anisotropy of ErIA-labeled SERCA, in the absence of ATP and Ca (Figure 1), was qualitatively similar to that of the ErITC-labeled enzyme—multiexponential decay in the microsecond time range with a nonzero final anisotropy at times greater than 500 μs (*10*). Three exponentials (eq 3, $n = 3$) were found to be necessary and sufficient to describe the anisotropy decay, based on evaluation of χ^2 values and nonrandom residual plots (Figure 1). The slight residual error (less than 0.0005, corresponding to less than 0.5% of $r_o = 0.102$) was not improved by increasing to a four-exponential function (eq 3, $n = 4$). However, as described in the tables below, the statistical errors (SEM) for amplitude values in fits are all greater than 0.0005. Because residuals for model-dependent fits described below were all at least as good as in Figure 1, we conclude that the SEM values given in the tables are reliable estimates of uncertainties.

Consistent with multiple rotational species in the system, the correlation times (ϕ_i in eq 3) ranged from 18 to 500 μs (Table 1), comparable to those obtained previously with

Table 1: Anisotropy Parameters from Model-Independent Fits[a]

sample	ϕ_1	ϕ_2	ϕ_3	r_1	r_2	r_3	r_∞	r_o
+Ca	19.9 (0.66)	147 (6)	446 (34)	0.014 (0.001)	0.028 (0.003)	0.024 (0.003)	0.041 (0.001)	0.107 (0.001)
−Ca	19.3 (0.37)	142 (5)	489 (30)	0.012 (0.003)	0.026 (0.009)	0.021 (0.002)	0.043 (0.002)	0.102 (0.001)
+Ca + ATP	18.0 (0.29)	131 (8)	460 (71)	0.010 (0.002)	0.024 (0.004)	0.015 (0.003)	0.047 (0.003)	0.096 (0.001)
−Ca + ATP	17.9 (0.08)	140 (3)	410 (32)	0.010 (0.003)	0.018 (0.002)	0.010 (0.002)	0.053 (0.002)	0.091 (0.004)

[a] TPA decays from ErIA-SR (Figure 2) were fit by a sum of exponentials plus a constant (eq 3, $n = 3$). ϕ_i values are rotational correlation times with fraction r_i. Fitting started at 5 μs after excitation. Each parameter is the average of four measurements of three different experiments, with the SEM given in parentheses.

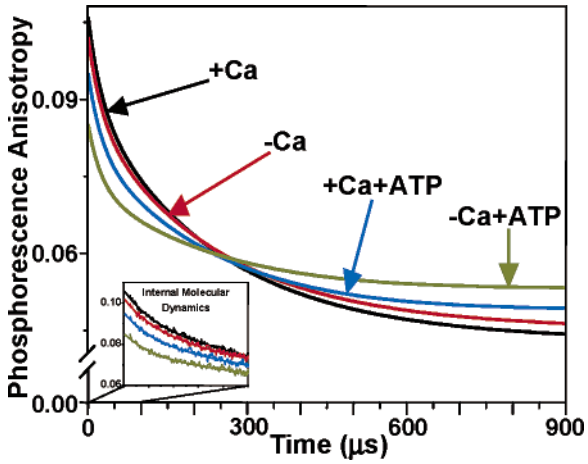

FIGURE 2: Effects of ATP and Ca on TPA of ErIA-SERCA. TPA was performed with 0.25 ± 0.05 mg/mL SERCA at 4 °C, in standard TPA buffer (pH 7.0). TPA decays represent 10 mM Ca (+Ca, black), no Ca (−Ca, red), 10 mM Ca and 1.0 mM ATP (+Ca + ATP, blue), and no Ca and 1.0 mM ATP (−Ca + ATP, green). For the sake of clarity, curves shown in the main plot are best fits from Table 1, while the inset shows data for the first 100 μs. Residuals indicated an excellent fit.

ErITC (*10*). The initial anisotropy value r_o was 0.102, significantly less than the rigid limit value of $r_{max} = 0.205$ (*26*), implying substantial submicrosecond internal molecular dynamics, characterized by the order parameter $S = (r_o/r_{max})^{1/2} = 0.71$ (eq 4), corresponding to an angular amplitude of $\theta_c = 38°$. We measured the anisotropy with 0.75−1.25 mol of ErIA bound per mole SERCA and found no variation in the anisotropy decay, which indicates that heterogeneous labeling and resonance energy transfer can be ruled out as affecting the anisotropy data.

Effects of ATP and Ca. A steady state ATPase reaction was initiated by the addition of ATP, Ca, and ionophore and was maintained at 4 °C during TPA data acquisition, allowing us to probe molecular dynamics during active calcium transport (Figure 2, +Ca + ATP). The initial anisotropy r_o decreased in the presence of Ca and ATP (implying increased amplitude of submicrosecond internal motion), and the final anisotropy r_∞ increased (implying either increased large-scale aggregation or a change in probe orientation toward the membrane normal) as compared to the decay in the absence of both ligands (−Ca). The Ca and ATP effects were opposite: ATP decreased r_o and increased r_∞, while Ca increased r_o and decreased r_∞. The decay obtained in the presence of both ligands suggests that the effects of Ca and ATP are additive or at least that one does not preclude occurrence of the other.

Under all tested conditions, three exponentials were necessary and sufficient to fit the anisotropy decay of ErIA-labeled SERCA (Table 1). Correlation times were not significantly affected by Ca or ATP, suggesting that sizes and shapes of rotating structures were not changed; the most significant changes were in initial and final anisotropies (r_o and r_∞). The initial anisotropy r_o was always substantially lower than the rigid limit value for ErIA of 0.205, indicating that order parameter S (eq 4) is less than 1 due to the presence of significant submicrosecond dynamics, which probably corresponds to flexibility within the SERCA P domain to which the ErIA probe is bound. Ca increased r_o and decreased r_∞, both in the presence and absence of ATP. ATP had larger effects than Ca, in the opposite directions: ATP decreased r_o and increased r_∞, whether Ca was present or not. The opposite effects on r_o and r_∞ produce a striking crossover of the decays near 300 μs (Figure 2).

The effects on r_o imply that ATP induces internal molecular dynamics within the pump on the time scale of a few microseconds or faster, while Ca restricts these motions partially. The first few microseconds of decay showed clear evidence for ATP-induced motions with a correlation time on the order of 1 μs, but this was comparable to the gating time of the detector, so a reliable correlation time could not be extracted from the data in this time range. Instead, we fitted the data starting at 5 μs after the exciting pulse, so the order parameter S, derived from r_o, reflects the amplitude of all motions with correlation times of less than 5 μs. The effects on r_∞ cannot be interpreted without a more explicit molecular model. We therefore analyzed the data using the model of uniaxial rotational diffusion (Table 2), which has been used previously to describe TPA decays in SR (*10*, *25*).

Model-Dependent Analysis: Uniaxial Diffusion. In this model (*10*, *25*), each species (different-sized aggregate, with mole fraction x_i) rotates globally about an axis perpendicular to the membrane with a characteristic diffusion coefficient D_i (eq 6) that is inversely proportional to its intramembrane volume (eq 9). A SERCA monomer is expected to have D of approximately 10^4/s at 4 °C (*10*); anything less suggests oligomerization. Given sufficient signal/noise, it is possible to determine independently the number (n in eq 6), sizes (proportional to $1/D_i$), and mole fractions (x_i) of these complexes, the fraction of aggregates that are so large as to be completely immobile (x_I), the tilt of the labeled domain with respect to the membrane (θ_a, θ_e), and the amplitude of its submicrosecond dynamics (θ_c). In practice, it is usually necessary to constrain the model with other information in order to obtain reliable conclusions. For example, if there is good evidence that a parameter has the same value for all data sets, this can be specified by linking that parameter in global analysis.

For each of the four Ca and ATP conditions used (Figure 2), an optimal fit required two uniaxially rotating components (eq 6, $n = 2$) and a substantial submicrosecond wobble ($\theta_c > 0$, i.e., $S < 1$). The first set of fits was performed allowing

Table 2: Parameters from Unconstrained, Model-Dependent Fits (Uniaxial Diffusion)[a]

	S	θ_c	D_1	D_2	x_1	x_2	x_I	θ_a	θ_e	χ^2
+Ca	0.71 (0.01)	37.3 (0.9)	8100 (500)	1010 (90)	0.28 (0.03)	0.72 (0.04)	0.00 (0.02)	14.8 (0.8)	45.8 (1.1)	0.96 (0.1)
−Ca	0.709 (0.01)	38.3 (0.9)	7400 (800)	1000 (120)	0.28 (0.02)	0.68 (0.05)	0.04 (0.02)	11.8 (0.7)	45.9 (1.3)	0.92 (0.05)
+Ca + ATP	0.68 (0.01)	39.9 (0.9)	11600 (3100)	1160 (130)	0.25 (0.08)	0.73 (0.08)	0.02 (0.08)	25.1 (1.0)	40.7 (1.4)	0.99 (0.10)
−Ca + ATP	0.65 (0.02)	42.0 (1.1)	12800 (3600)	1200 (120)	0.32 (0.03)	0.68 (0.04)	0.00 (0.02)	23.0 (1.3)	38.5 (1.6)	0.92 (0.11)

[a] TPA decays were fit by the uniaxial diffusion model (eq 6). S is the order parameter for submicrosecond motion with a half-cone angle θ_c (°), calculated using eq 5. D_1 and D_2 are diffusion coefficients (s^{-1}) with fractions x_1 and x_2, respectively. The values of θ_e (°) and θ_a (°) are angles of emission and absorption dipoles with respect to the membrane normal [δ, the angle between dipoles, was set to 34.8°; see ref (*26*)]. Each parameter is the average of four measurements of three experiments, with the SEM given in parentheses.

Table 3: Parameters from Constrained, Model-Dependent Fits (Uniaxial Diffusion)[a]

sample	S	θ_c	θ_a	θ_e	χ^2
+Ca	0.722 (0.006)	36.7 (0.7)	12.1 (0.2)	46.2 (0.5)	0.74 (0.08)
−Ca	0.706 (0.004)	37.9 (0.6)	11.6 (0.3)	45.5 (0.3)	0.96 (0.1)
+Ca + ATP	0.684 (0.003)	39.5 (0.6)	31.9 (0.2)	36.5 (0.2)	0.93 (0.1)
−Ca + ATP	0.663 (0.004)	41.0 (0.7)	31.0 (0.7)	38.8 (1.2)	0.87 (0.09)

[a] TPA decays were globally fit by the uniaxial diffusion model (eq 6). S is the order parameter for submicrosecond motion with a half-cone angle θ_c (°), calculated using eq 5. The immobile fraction x_I was assumed to be zero. Rotational diffusion coefficients and corresponding fractions were linked for global fitting, giving values $D_1 = 0.98 \times 10^4$ s^{-1}; $x_1 = 0.28$; $D_2 = 1.05 \times 10^3$ s^{-1}; and $x_2 = 0.72$. θ_e (°) and θ_a (°) are angles of emission and absorption dipoles with respect to the membrane normal. Fitting started 5 μs after excitation. Each parameter is the average of four measurements of three experiments, with the SEM given in parentheses.

all parameters to vary ("unconstrained"; Table 2). The immobile fraction x_I returned by the fit was less than 5% for all four cases. Thus, there are virtually no large-scale aggregates that rotate slower than the microsecond time scale, as concluded previously for SR labeled with ErITC (*10*). The final anisotropy, which varies substantially among the four data sets (Table 1), depends only on x_I and the probe tilt (θ_a, θ_e), so the change in final anisotropy r_∞ must be due to a change in the probe (domain) tilt, not to a change in large-scale aggregation. The two diffusion coefficients (D_1 and D_2) differed by approximately 1 order of magnitude (Table 2), but their values and mole fractions (x_1 and x_2) were virtually unchanged (variation of 25% or less, with no significant change in χ^2) over the four sets of conditions (Figure 2). This indicates that there are no significant changes in SERCA self-association as a function of Ca and ATP, as concluded from our previous saturation transfer EPR study of spin-labeled SERCA (*30*). Therefore, to constrain the fit sufficiently to obtain reliable results, we performed a global analysis in which the diffusion coefficients and their mole fractions were linked (assumed to be the same for all four conditions), and the immobile fraction x_I was set to 0 ("constrained"; Table 3). The resulting analysis returned fits (judged by residuals and χ^2 values) that were as good as the unconstrained fits (Table 2). This analysis indicates that the ligands ATP and Ca primarily affect intramolecular dynamics and not oligomeric interactions.

The constrained fits using the uniaxial rotational motion model showed that only two rotating species, order parameter S, and probe tilt angles were sufficient to fit the data well. A change in oligomeric size or immobile fraction could not account for the changes observed, consistent with our previous observations (*30*). Upon removal of Ca, fits showed only a minimal decrease in S, indicating that this ligand may slow intramolecular motion. No change was observed in probe angle parameters (domain tilt) upon removal of Ca. A significant change in intramolecular dynamics was observed upon addition of ATP. The order parameter decreased by approximately 20%, which indicates that motions in the phosphorylation domain are induced by nucleotide, rather than Ca binding.

Domain Tilt. Data analysis, which included probe angles of absorption and emission dipoles relative to the membrane normal, revealed that these angles change significantly upon addition of nucleotide (Table 3) by approximately 20°. The largest change was in θ_a, which increased from 12 to 31° upon addition of nucleotide. This change was sufficient to account for the crossover, and the data could be well-described without a change in SERCA oligomeric state. Nucleotide effects on probe tilt were dominant over those of Ca. In the presence of nucleotide, θ_a was always approximately 20° greater than in the absence of nucleotide, whether Ca was present or not. This indicates that the P domain, to which this probe is bound rigidly, is tilting upon binding of ATP by at least 20°. Crystallographic data predict a similar tilt in the P domain (*2*, *3*). However, a striking difference between the crystallographic results and our spectroscopic results is that the two crystal structures differ primarily in the presence and absence of Ca, while the TPA data reports change in tilt upon ATP addition but not upon Ca addition.

Effect of Nucleotide Analogues. Several other nucleotides were tested in order to determine which moiety in the ATP molecule was responsible for increased intramolecular motion as well as domain tilt. We found that ADP induced a similar but smaller change in anisotropy, while AMP, GTP, or acetyl phosphate did not show any effect (data not shown). Therefore, the nucleotide effect is specific for the adenylyl moiety and at least two phosphate groups, and the full effect requires three phosphate groups. AMPPCP, a nonhydrolyzable ATP analogue, caused essentially the same anisotropy effects (Figure 3) as ATP (Figure 2). Upon addition of AMPPCP, initial anisotropy was decreased, indicating more intramolecular motion. Thus, the ATP effect is due to nucleotide binding, and not to nucleotide hydrolysis and formation of a phosphoenzyme intermediate. These results indicate that the tilt of the P domain is sensitive to both Ca and ATP binding but insensitive to ATP hydrolysis and phosphoenzyme formation.

Melittin-Induced Aggregation. Melittin has been shown to induce SERCA self-aggregation and concomitant enzyme inhibition (*15*, *31*−*33*), so we used melittin to explore the functional coupling between internal and global dynamics in SERCA. Anisotropy decays of ErIA-labeled SERCA were very sensitive to the addition of melittin (Figure 4); both

Table 4: Parameters from Unconstrained, Model-Dependent Fits (Uniaxial Diffusion, as in Table 2) of ErIA-SR, as Affected by Melittin and/or AMPPCP[a]

melittin/ SERCA (mol)	S	θ_c	D_1	D_2	x_1	x_2	x_I	θ_a	θ_e	χ^2
0	0.71 (0.01)	37.3 (0.9)	8850 (490)	1066 (95)	0.26 (0.03)	0.74 (0.03)	0.0 (0.0)	12.0 (0.8)	44.7 (1.1)	0.96 (0.1)
5	0.70 (0.01)	37.8 (0.9)	1060 (80)	227 (24)	0.61 (0.05)	0.39 (0.05)	0.0 (0.0)	11.1 (0.7)	42.5 (1.3)	0.92 (0.05)
10	0.71 (0.01)	37.8 (0.7)	1051 (108)	248 (26)	0.36 (0.08)	0.20 (0.08)	0.44 (0.08)	12.2 (1.0)	42.7 (1.4)	0.99 (0.10)
0 + AMPPCP	0.65 (0.02)	42.5 (1.1)	9900 (580)	1046 (120)	0.22 (0.03)	0.78 (0.03)	0.0 (0.0)	31.1 (1.3)	34.5 (1.6)	0.92 (0.11)
5 + AMPPCP	0.70 (0.01)	38.3 (0.9)	1043 (112)	237 (21)	0.56 (0.02)	0.41 (0.02)	0.03 (0.02)	12.3 (0.8)	44.5 (1.9)	0.96 (0.08)

[a] TPA decays were fit to the uniaxial diffusion model (eq 6). *S* is the order parameter for submicrosecond motion with a half-cone angle θ_c (°), calculated using eq 5. D_1 and D_2 are rotational diffusion coefficients (s^{-1}) with mole fractions x_1 and x_2, respectively. The values of θ_e (°) and θ_a (°) are angles of emission and absorption dipoles with respect to the membrane normal. The angle between dipoles (δ) was set to 34.8°; see ref (*26*). Fitting started 5 μs after excitation. Each parameter is the average of four measurements on each of three experiments (SEM in parentheses).

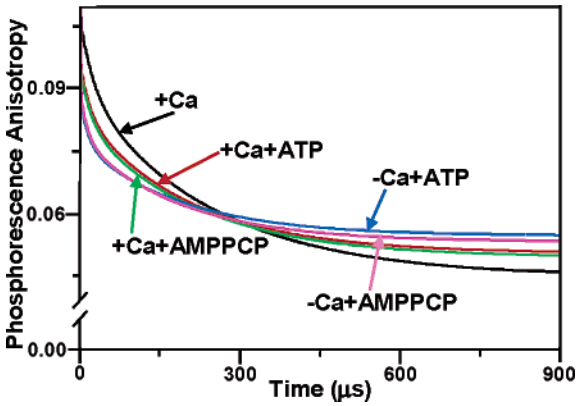

FIGURE 3: Effects of AMPPCP and ATP on TPA of ErIA-SERCA. TPA was performed as in Figure 2, except that curves labeled AMPPCP contained 1.0 mM AMPPCP instead of ATP. For the sake of clarity, curves shown are best fits of eq 3. Fitting results for AMPPCP are shown in Table 4.

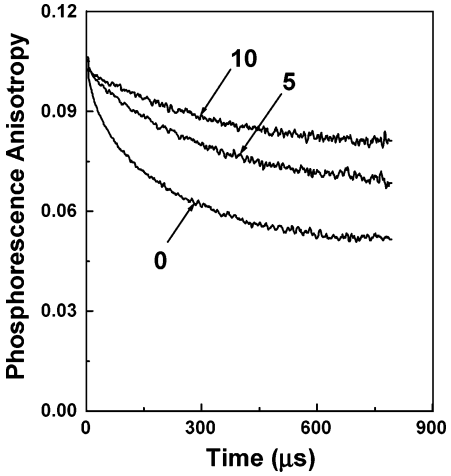

FIGURE 4: Melittin-induced aggregation. TPA was performed with 0.25 ± 0.05 mg/mL SERCA at 4 °C in standard TPA buffer (pH 7.0) and 0.103 mM $CaCl_2$ to furnish 10 mM free Ca. The decays represent no melittin and 5 and 10 mol of melittin per mole SERCA (0, 5, and 10, respectively). Fitting results are shown in Table 4.

the rate and the amplitude of anisotropy increased dramatically, consistent with previous results with ErITC indicating large-scale aggregation of SERCA due to melittin (*15*). Analysis of anisotropy decays (Table 4) confirmed the conclusion that, in contrast to the effects of nucleotides and Ca (Figures 2 and 3 and Table 3), melittin clearly induces self-association of SERCA. At 5 melittin/SERCA, the smallest rotating species ($D_i \sim 10^4$ s^{-1}) disappeared in favor of a very large rotating species ($D_i \sim 250$ s^{-1}), probably corresponding to large SERCA aggregates, and upon addition

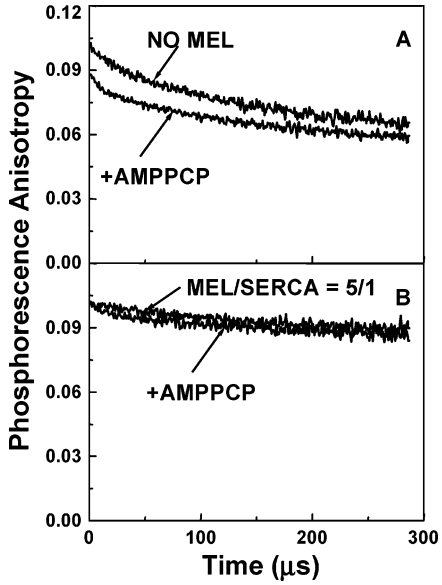

FIGURE 5: Melittin modulates the AMPPCP-induced internal dynamics in the P domain. The decays represent an AMPPCP-induced decrease of rapid anisotropy in the absence (A) and presence of 5 mol of melittin per mole of SERCA (B). The rapid anisotropy change is eliminated by melittin-induced aggregation of the enzyme. Fitting parameters are shown in Table 4.

of 10 melittin/SERCA, the immobile fraction increased from 0 to 0.44, indicating that the aggregates had become too large to detect by TPA (Table 4).

Intramolecular Motion Inhibited by Melittin. We used melittin to determine the effects of SERCA aggregation on the nucleotide-induced internal molecular dynamics detected by ErIA (Figure 5 and Table 4, bottom). In the presence of AMPPCP, melittin caused a substantial increase in anisotropy, consistent with the large-scale aggregation induced in the absence of AMPPCP. More importantly, this SERCA aggregation resulted in the complete reversal of the structural dynamics induced by AMPPCP (Figure 5, bottom; Table 4, bottom); both the submicrosecond-order parameter *S* and the probe tile angle θ_a returned to the prenucleotide levels. We conclude that SERCA aggregation by melittin constricts the intramolecular dynamics of the enzyme, preventing the functionally important dynamic effects of ATP.

DISCUSSION

Summary of Results. We have investigated SERCA molecular dynamics using the phosphorescent probe ErIA, which is bound to the P domain and minimally interferes with the enzyme's calcium-dependent ATPase activity. This

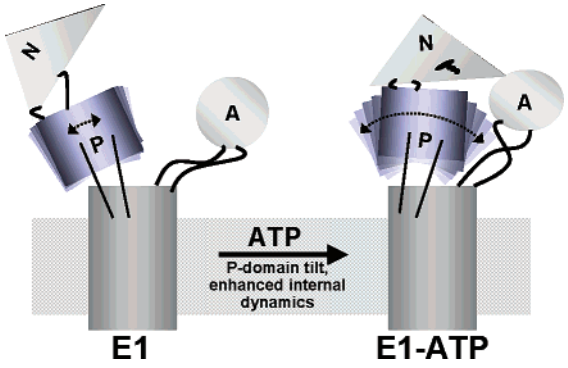

FIGURE 6: Model for the effect of ATP binding on the structural dynamics of SERCA, based on the crystal structures (see text) and on the TPA data in this study. ATP binds to the nucleotide-binding domain (N) and has two effects on the phosphorylation domain (P): a tilt of at least 20° (shown by TPA; crystal structures show this change upon Ca release) and increased internal dynamics (shown by TPA). Other changes depicted are based on the crystal structures: the N domain is shown to clamp down in order to bring ATP closer to the phosphorylation site on the P domain, and the actuator domain (A) also undergoes significant motion. No attempt is made to depict changes within the transmembrane domain.

allowed us to detect molecular dynamics during active Ca pumping. Our results show that ATP binding induces substantial changes in the structure and dynamics of the P domain (Figure 6), while Ca binding has very little effect. When SERCA is aggregated and inhibited by melittin, these ATP-induced structural changes are prevented, indicating a coupling between internal dynamics, SERCA self-association, and function.

Relationship to SERCA Crystal Structures. X-ray structures have been obtained from frozen crystals of SERCA−detergent mixtures in the presence of either mM Ca [designated E1(Ca)] or the inhibitor thapsigargin [designated E2(Tg)] (*2*, *3*). It has been proposed that the dramatic differences between these two crystal structures correspond to the changes induced by release of micromolar Ca under physiological conditions. In the P domain, the most significant change predicted by these two structures is a tilt of 20−30° relative to the membrane normal. Indeed, our TPA data, recorded under physiological conditions, confirm that the P domain tilts by at least 20°, but this structural change is induced by ATP binding, not by Ca removal (Table 3, see changes in θ_a). A more recent report using SERCA crystallography (*34*) attributes a major structural change in the SERCA cytoplasmic domains in the presence of Ca to the binding of nucleotide. Although this study describes a tilt of the N domain with respect to the P domain, it supports our finding that nucleotide binding leads to a significant structural rearrangement and increased molecular dynamics within the cytoplasmic domains of SERCA and that Ca binding has comparatively minor effects. Therefore, our revised model in Figure 6 depicts essentially the same protein structural changes predicted on the basis of the E1(Ca) and E2(Tg) crystal structures but shows the transition as one between E1 and E1-ATP. An ATP-dependent structural change in SERCA was detected previously using iodoacetamide spin-labeled SR (*16*, *17*). Of course, we cannot rule out that the tilt of the probe detected by TPA is due to some internal rearrangement within the P domain, rather than a tilt of the entire domain. In addition to the tilt of the P domain, the model shows a previously undetected increase in the amplitude of internal molecular dynamics of this domain, based on the observed decrease in initial phosphorescence anisotropy (decreased *S* in Table 3).

How might these changes in structural dynamics be involved in the enzyme's mechanism? Part of this answer comes from the observed effects of melittin (discussed below), and part of the explanation is suggested by inspection of the crystal structure data. The distance from the nucleotide binding site in the N domain (K515) to the autophosphorylated residue (D351) does not change significantly between the two crystal structures [distance in E1(Ca) ∼ 30 Å vs E2(Tg) ∼ 28 Å]. In neither of the two structures would the γ-phosphoryl group of ATP be close enough to D351 for phosphate transfer to occur. Both the E1(Ca) and the E2(Tg) crystal structures are merely snapshots, recorded in frozen crystals. It is likely that additional molecular motions are needed for actual catalysis to occur. Thus, it is possible that the internal dynamics of the P domain, detected by our TPA measurements but not by crystallography, can account for the difference in distance required to bring the two sites close enough for phosphoryl transfer to occur. The two domains may come into contact transiently, through fast internal dynamics, long enough for transfer of the phosphoryl group to occur. After phosphoryl transfer, the two domains may remain transiently in this dynamic state, in the ADP sensitive phosphoenzyme conformation that is easily reversed, but then return to a more static state (ADP insensitive) to prevent reversal of the reaction. We noted that ADP induced a much smaller TPA change than ATP.

It has been shown that the ATP polyphosphate chain exists in a folded configuration so that it approximates SERCA residue T441 (Hua, 2002 #99). The phosphorylated residue, SERCA D351, is approximated only in an energetically unfavorable conformation of the ATP molecule due to repulsion between the terminal phosphate group and D351 (Ma, 2003 #101; Inesi, 2004 #100). The transient approach of the terminal phosphate group on the phosphorylated residue, due to internal molecular dynamics of SERCA detected by TPA, may be needed for phosphoryl transfer to occur and to prevent the enzyme from having to exist in an energetically unfavorable state.

The effect of the nucleotide on the P domain may in part be due to translation of molecular dynamics and motions from the N domain. However, it can also be explained based on evidence that a number of residues in the P domain itself are involved in and crucial for binding of nucleotide (*35*).

Relationship to Previous Spectroscopic Studies. Analysis of anisotropy effects showed that AMPPCP, a nonhydrolyzable ATP analogue, induced the same anisotropy changes as ATP. This indicates that the nucleotide effect occurs at the binding step, prior to hydrolysis and transfer of a phosphoryl group to the enzyme. The addition of Ca had much smaller effects on SERCA molecular dynamics, in the opposite direction to those induced by nucleotide. These results are in agreement with previous EPR data, showing that AMPPCP has a greater effect than Ca on nanosecond spin label dynamics at Cys 674 (*17*, *36*), and that neither of these ligands affects global dynamics (oligomeric state) (*30*). In support of rearrangement of the probe dipole orientation with respect to the membrane (changes in θ_a and θ_e indicating domain tilt) or increased internal molecular dynamics (decrease in order parameter *S*), other studies have provided

evidence for structural flexibility in the cytoplasmic domains of SERCA (*3*, *6*, *37*, *38*). Previous TPA studies of an ErITC probe on the N domain of SERCA did not detect any effect of Ca or ATP (*10*, *39*), while a previous frequency domain phosphorescence study of ErITC attached to another site on the N domain reported increased dynamics with Ca but not with ATP (*40*).

Structural models of SERCA transitions during the catalytic cycle have been proposed (*3*, *6*) in which Ca binding elicits conformational changes in both the transmembrane and the cytoplasmic domains. In contrast, our data suggest that the motions of the P domain, as reported by ErIA, are not greatly influenced by the binding of Ca alone, despite the requirement of Ca for catalysis (*1*). Our data support a reaction model in which both Ca- and ATP-induced motions are required for calcium-dependent ATPase activity. We propose that ATP binding leads to increased motion within the cytoplasmic domains, eliciting the motions required to bring the nucleotide binding and phosphorylation sites into proximity so that autophosphorylation and Ca translocation may occur, while enzyme dephosphorylation and Ca binding make the cytoplasmic domains available for a new cycle of catalytic activity.

Global Rotational Motion Coupled to Internal Molecular Dynamics. Melittin inhibits SERCA by inducing the formation of large oligomers (*15*, *31*, *33*) due primarily to electrostatic interactions (*32*). This is manifested in our TPA data by formation of larger rotating species and by the appearance of an immobile fraction, neither of which was observed in the absence of melittin (Table 4). Thus, ErIA reports simultaneously the internal molecular dynamics of the active enzyme, as well as global rotational motion that is sensitive to the oligomeric state. Melittin-induced SERCA aggregation, which inactivates the enzyme, abolishes nucleotide-induced internal molecular dynamics as well as the changes in P domain tilt, supporting the proposal that functional dynamics motion within the enzyme is coupled to SERCA global motion and self-association. A similar mechanism of inhibition probably governs the inhibitory interaction of phospholamban and SERCA in the heart, since SERCA inhibition by phospholamban is accompanied by SERCA aggregation (*39*, *41*).

Conclusions. The internal molecular dynamics of ErIA-labeled SERCA, detected in the P domain during active calcium pumping, is affected dramatically by ATP but only slightly by Ca. ATP binding causes a substantial tilt of the P domain, suggesting that the ATP-bound state in solution is similar to the crystal structure obtained in the presence of thapsigargin, and induces an increase in submicrosecond internal dynamics. These changes in protein dynamics are functionally important, as evidenced by melittin-induced inhibition of both enzyme activity and ATP-induced changes in internal dynamics, correlated with enzyme self-association. We propose that functional coupling between oligomeric interactions and internal dynamics plays an important part in regulation of SERCA activity and may be involved in the regulation of SERCA by phospholamban and other regulatory factors.

ACKNOWLEDGMENT

We thank Joseph Mersol and James Mahaney for excellent advice and Octavian Cornea for technical assistance.

REFERENCES

1. Inesi, G. (1985) Mechanism of calcium transport, *Annu. Rev. Physiol. 47*, 573−601.
2. Toyoshima, C., Nakasako, M., Nomura, H., and Ogawa, H. (2000) Crystal structure of the calcium pump of sarcoplasmic reticulum at 2.6 A resolution, *Nature 405*, 647−655.
3. Toyoshima, C., and Nomura, H. (2002) Structural changes in the calcium pump accompanying the dissociation of calcium, *Nature 418*, 605−611.
4. Stokes, D. L., Auer, M., Zhang, P., and Kuhlbrandt, W. (1999) Comparison of H+-ATPase and Ca2+-ATPase suggests that a large conformational change initiates P-type ion pump reaction cycles, *Curr. Biol. 9*, 672−679.
5. Lee, A. G. (2002) Ca(2+)-ATPase structure in the E1 and E2 conformations: Mechanism, helix-helix and helix-lipid interactions, *Biochim. Biophys. Acta 1565*, 246−266.
6. Xu, C., Rice, W. J., He, W., and Stokes, D. L. (2002) A structural model for the catalytic cycle of Ca(2+)-ATPase, *J. Mol. Biol. 316*, 201−211.
7. Jona, I., and Martonosi, A. (1991) The effect of high pressure on the conformation, interactions and activity of the Ca(2+)-ATPase of sarcoplasmic reticulum, *Biochim. Biophys. Acta 1070*, 355−373.
8. Stokes, D. L., and Lacapere, J. J. (1994) Conformation of Ca(2+)-ATPase in two crystal forms. Effects of Ca2+, thapsigargin, adenosine 5′-(β,γ-methylene)triphosphate), and chromium(III)-ATP on crystallization, *J. Biol. Chem. 269*, 11606−11613.
9. Kutchai, H., Geddis, L. M., Jones, L. R., and Thomas, D. D. (1998) Differential effects of general anesthetics on the quaternary structure of the Ca-ATPases of cardiac and skeletal sarcoplasmic reticulum, *Biochemistry 37*, 2410−2421.
10. Birmachu, W., and Thomas, D. D. (1990) Rotational dynamics of the Ca-ATPase in sarcoplasmic reticulum studied by time-resolved phosphorescence anisotropy, *Biochemistry 29*, 3904−3914.
11. Karon, B. S., Mahaney, J. E., and Thomas, D. D. (1994) Halothane and cyclopiazonic acid modulate Ca-ATPase oligomeric state and function in sarcoplasmic reticulum, *Biochemistry 33*, 13928−13937.
12. Kutchai, H., Mahaney, J. E., Geddis, L. M., and Thomas, D. D. (1994) Hexanol and lidocaine affect the oligomeric state of the Ca-ATPase of sarcoplasmic reticulum, *Biochemistry 33*, 13208−13222.
13. Birmachu, W., Voss, J. C., Louis, C. F., and Thomas, D. D. (1993) Protein and lipid rotational dynamics in cardiac and skeletal sarcoplasmic reticulum detected by EPR and phosphorescence anisotropy, *Biochemistry 32*, 9445−9453.
14. Karon, B. S., and Thomas, D. D. (1993) Molecular mechanism of Ca-ATPase activation by halothane in sarcoplasmic reticulum, *Biochemistry 32*, 7503−7511.
15. Voss, J., Birmachu, W., Hussey, D. M., and Thomas, D. D. (1991) Effects of melittin on molecular dynamics and Ca-ATPase activity in sarcoplasmic reticulum membranes: Time-resolved optical anisotropy, *Biochemistry 30*, 7498−7506.
16. Landgraf, W. C., and Inesi, G. (1969) ATP dependent conformational change in "spin labelled" sarcoplasmic reticulum, *Arch. Biochem. Biophys. 130*, 111−118.
17. Lewis, S. M., and Thomas, D. D. (1992) Resolved conformational states of spin-labeled Ca-ATPase during the enzymatic cycle, *Biochemistry 31*, 7381−7389.
18. Speirs, A., Moore, C. H., Boxer, D. H., and Garland, P. B. (1983) Segmental motion and rotational diffusion of the Ca2+-translocating adenosine triphosphatase of sarcoplasmic reticulum, measured by time-resolved phosphorescence depolarization, *Biochem. J. 213*, 67−74.
19. Fernandez, J. L., Rosemblatt, M., and Hidalgo, C. (1980) Highly purified sarcoplasmic reticulum vesicles are devoid of Ca2+-independent ('basal') ATPase activity, *Biochim. Biophys. Acta 599*, 552−568.
20. Birmachu, W., Nisswandt, F. L., and Thomas, D. D. (1989) Conformational transitions in the calcium adenosinetriphosphatase studied by time-resolved fluorescence resonance energy transfer, *Biochemistry 28*, 3940−3947.
21. Gornall, A. G., Bardawill, C. J., and David, M. M. (1948) Determination of serum proteins by means of the biuret reaction, *J. Biol. Chem. 177*, 751−766.
22. Reddy, L. G., Cornea, R. L., Winters, D. L., McKenna, E., and Thomas, D. D. (2003) Defining the molecular components of

calcium transport regulation in a reconstituted membrane system, *Biochemistry 42*, 4585−4592.
23. Ludescher, R. D., and Thomas, D. D. (1988) Microsecond rotational dynamics of phosphorescent-labeled muscle cross-bridges, *Biochemistry 27*, 3343−3351.
24. Fabiato, A. (1988) Computer programs for calculating total from specified free or free from specified total ionic concentrations in aqueous solutions containing multiple metals and ligands, *Methods Enzymol 157*, 378−417.
25. Mersol, J. V., Kutchai, H., Mahaney, J. E., and Thomas, D. D. (1995) Self-association accompanies inhibition of Ca-ATPase by thapsigargin, *Biophys. J. 68*, 208−215.
26. Prochniewicz, E., Zhang, Q., Howard, E. C., and Thomas, D. D. (1996) Microsecond rotational dynamics of actin: Spectroscopic detection and theoretical simulation, *J. Mol. Biol. 255*, 446−457.
27. Szabo, A. (1984) Theory of fluorescence depolarization in macromolecules and membranes, *J. Chem. Phys. 81*, 150−167.
28. Suzuki, H., Obara, M., Kubo, K., and Kanazawa, T. (1989) Changes in the steady-state fluorescence anisotropy of N-iodoacetyl-N′-(5-sulfo-1-naphthyl)ethylenediamine attached to the specific thiol of sarcoplasmic reticulum Ca2+-ATPase throughout the catalytic cycle, *J. Biol. Chem. 264*, 920−927.
29. Mueller, B., Karim, C. B., Negrashov, I. V., Kutchai, H., and Thomas, D. D. (2004) Direct detection of phospholamban and SERCA interaction in membranes using fluroescence resonance energy transfer. *Biochemistry 43*, 8754−8765.
30. Lewis, S. M., and Thomas, D. D. (1991) Microsecond rotational dynamics of spin-labeled Ca-ATPase during enzymatic cycling initiated by photolysis of caged ATP, *Biochemistry 30*, 8331−8339.
31. Mahaney, J. E., Kleinschmidt, J., Marsh, D., and Thomas, D. D. (1992) Effects of melittin on lipid−protein interactions in sarcoplasmic reticulum membranes, *Biophys. J. 63*, 1513−1522.
32. Voss, J. C., Mahaney, J. E., and Thomas, D. D. (1995) Mechanism of Ca-ATPase inhibition by melittin in skeletal sarcoplasmic reticulum, *Biochemistry 34*, 930−939.
33. Shorina, E. A., Mast, N. V., Storey, K. B., Lopina, O. D., and Rubtsov, A. M. (1999) Characteristics of the interaction of melittin with sarcoplasmic reticulum membranes, *Biochemistry (Moscow) 64*, 705−713.
34. Sorensen, T. L., Moller, J. V., and Nissen, P. (2004) Phosphoryl transfer and calcium ion occlusion in the calcium pump, *Science 304*, 1672−165.
35. McIntosh, D. B., Clausen, J. D., Woolley, D. G., MacLennan, D. H., Vilsen, B., and Andersen, J. P. (2003) ATP binding residues of sarcoplasmic reticulum Ca2+-ATPase, *Ann. N. Y. Acad. Sci. 986*, 101−105.
36. Mahaney, J. E., Froechlich, J. P., and Thomas, D. D. (1995) Conformational transitions of the sarcoplasmic reticulum Ca-ATPase studied by time-resolved EPR and quenched-flow kinetics, *Biochemistry 34*, 4864−7489.
37. Suzuki, S., Kawato, S., Kouyama, T., Kinosita, K., Jr., Ikegami, A., and Kawakita, M. (1989) Independent flexible motion of submolecular domains of the Ca2+, Mg2+- ATPase of sarcoplasmic reticulum measured by time-resolved fluorescence depolarization of site-specifically attached probes, *Biochemistry 28*, 7734−7740.
38. Restall, C. J., Coke, M., Murray, E. K., and Chapman, D. (1985) Conformational changes in the (Ca2+ + Mg2+)-ATPase of sarcoplasmic reticulum detected using phosphorescence polarization, *Biochim. Biophys. Acta 813*, 96−102.
39. Voss, J., Jones, L. R., and Thomas, D. D. (1994) The physical mechanism of calcium pump regulation in the heart, *Biophys. J. 67*, 190−196.
40. Huang, S., and Squier, T. C. (1998) Enhanced rotational dynamics of the phosphorylation domain of the Ca-ATPase upon calcium activation, *Biochemistry 37*, 18064−18073.
41. Thomas, D. D., Reddy, L. G., Karim, C. B., Li, M., Cornea, R., Autry, J. M., Jones, L. R., and Stamm, J. (1998) Direct spectroscopic detection of molecular dynamics and interactions of the calcium pump and phospholamban, *Ann. N. Y. Acad. Sci. 853*, 186−194.

BI0489457